PAPER

Angular dependence of the magnetic properties of permalloy and nickel nanowires as a function of their diameters

View the article online for updates and enhancements.

Materials Research Express

Angular dependence of the magnetic properties of permalloy and nickel nanowires as a function of their diameters

Sofía Raviolo[1], Felipe Tejo[2], Noelia Bajales[1,3] and Juan Escrig[2,4]

1 Universidad Nacional de Córdoba, FaMAF, 5000 Córdoba, Argentina
2 Departamento de Física, Universidad de Santiago de Chile, Usach, 9170124 Santiago, Chile
3 CONICET, IFEG, 5000 Córdoba, Argentina
4 Center for the Development of Nanoscience and Nanotechnology, 9170124 Santiago, Chile

E-mail: juan.escrig@usach.cl

Abstract

In this paper we have compared the angular dependence of the magnetic properties of permalloy ($Ni_{80}Fe_{20}$) and nickel nanowires by means of micromagnetic simulations. For each material we have chosen two diameters, 40 and 100 nm. Permalloy nanowires with smaller diameters ($d = 40$ nm) exhibit greater coercivity than nickel nanowires, regardless of the angle at which the external magnetic field is applied. In addition, both Py and Ni nanowires exhibit the same remanence values. However, the nanowires of larger diameters ($d = 100$ nm) exhibit a more complex behavior, noting that for small angles, nickel nanowires are those that now exhibit a greater coercivity in comparison to those of permalloy. The magnetization reversal modes vary as a function of the angle at which the external field is applied. When the field is applied parallel to the wire axis, it reverts through nucleation and propagation of domain walls, whereas when the field is applied perpendicular to the axis, it reverts by a pseudo-coherent rotation. These results may provide a guide to control the magnetic properties of nanowires for use in potential applications.

1. Introduction

Low-dimensional magnetic nanostructures are currently a subject of increasing interest due to their broad potential applications, ranging from high density recording media to biological cell manipulation [1–3]. A key issue for a successful development of nanoscopic devices is the understanding of the magnetic properties in high aspect ratio and quasi-one-dimensional features such as magnetic nanowires (mNWs) [4–6]. Recent investigations have shown that controlling domain walls (DW) in mNWs provide a route to store information [7] or perform logic functions [8]. Moreover, their functionalities from magnetothermopower and magnetoresistance characteristics at room temperature compete with those of conventional magnetoresistance and thermoelectric materials [9, 10]. These structures allow the resolution of basic physical questions about how the magnetization reversal mechanisms are strongly dependent on the geometry. Thus, with increasing diameter of mNWs, the shape anisotropy leads the equation governing the magnetization equilibrium [11]. Likewise, mNWs also provide tunable properties by varying the length, inter-wire distance and composition of a wide spectrum of different elements and their combinations, arising from shape anisotropy, magnetocrystalline anisotropy and magnetostatic interaction between NWs [12–14]. Recently, Singh *et al* [15] reported the effect of α-particle irradiation on the magnetic properties of Ni NWs arrays.

Amongst the most promising alloy NWs of industrial interest for high impact technology, soft magnetic materials such as permalloy ($Ni_{80}Fe_{20}$) structures are attractive candidates to be used as non-volatile data storage [16], due to their remarkable ferromagnetic properties, significant magnetization behavior and invar effect in certain compositions [17, 18]. Ramazani *et al* [19] have reported that by capturing the magnetic fingerprints of the NiFe NW arrays using the first-order reversal curve analysis, it was revealed that increasing length and

diameter increase the inter-wire magnetostatic interactions. Furthermore, Zhang *et al* [20] showed that the magnetic anisotropic properties of NiFe alloy nanowires, successfully fabricated in the pores of the anodized aluminum oxide, are strongly dependent on the length of NiFe alloy nanowires. Till date, permalloy NWs have been widely studied [11, 16, 21–23]; however, in one-dimensional devices the experimental analysis of DW motion is complicated because the available techniques are not able to jointly examine the wall structure and dynamics. Therefore, the lack of proper resolution has led to controversial results in the literature. In this framework, micromagnetic simulations are an ideal method for studying the wall motion in a mNW. There are some antecedents that show DW mobility in permalloy nanowires using micromagnetic simulations, for a large range of applied fields and nanowire cross sections [11, 22]. These studies reported that wall mobility decreases linearly up to the critical field because the dynamic DW length also decreases with increasing field strength. Additionally, Willcox *et al* [24] simulated a number of permalloy nanowires with geometric pinning sites and found key design limits and some interesting observations, such as the formation of vortex DWs with small separations, showing that symmetric pinning sites are preferential to asymmetric sites. Being permalloy NWs Ni-rich systems, the work carried out by Leighton *et al* [25] on the reversal processes of asymmetric Ni nanowires contributes to better understand NiFe NWs when the behavior of both systems, concerning the coercive field and remanence magnetization as a function of the geometry and the angle at which the field is applied, needs to be compared. However, there is no report that investigates in a comparative approach the angular and geometrical dependence of the magnetic properties in cylindrical permalloy ($Ni_{80}Fe_{20}$) and nickel nanowires.

In this paper, micromagnetic simulations have been performed in order to gain insight into the angular, diameter and composition dependences of the magnetic properties for 1 μm long cylindrical nanostructures with wire morphology. The behavior of the coercivity *Hc* and remanence *Mr*, as well as the magnetization reversal processes were explored, concluding that changing the angle θ at which the external magnetic field is applied enables us to control the magnetic properties of cylindrical nanowires.

2. Micromagnetic simulations

The magnetization dynamics is governed by the Landau–Lifshitz–Gilbert equation (LLG) [26]

$$\frac{d\vec{M}}{dt} = -\gamma \, \vec{M} \times \vec{H}_{\text{eff}} + \frac{\alpha}{M_s}\vec{M} \times \frac{d\vec{M}}{dt}, \qquad (1)$$

where γ is the gyromagnetic ratio of the free electron spin and α is a phenomenological damping constant. The equation describes both the precession and relaxation motion of the magnetization in an effective field $\vec{H}_{\text{eff}}$. The calculations were performed using Object Oriented MicroMagnetic Framework software [27], which uses an iterative process to solve the LLG equation for each cell of a finite element mesh [24].

The simulated nanowires were permalloy ($Ni_{80}Fe_{20}$) and nickel materials, each one of 1 μm long (*L*), with diameters $d = 40$ and 100 nm. For permalloy material, the exchange stiffness, *A*, was set at 13×10^{-12} J m^{-1}, and the material saturation magnetization, M_s, was set to 800×10^3 A m^{-1}, while for Ni material the numerical simulations were performed using the following parameters: saturation magnetization $Ms = 490 \times 10^3$ A m^{-1}, and exchange stiffness constant $A = 9 \times 10^{12}$ J m^{-1}. Polycrystalline samples were considered, so the magnetocrystalline anisotropy was not taken into account. The samples were discretized into a cell size of $2 \times 2 \times 5$ nm^3, where spins are free to rotate in three dimensions. The choice of the discretization scheme was validated by the fact that the numerical roughness (generated by the square mesh representation) can represent real roughness on the wire surface. The damping coefficient of the Landau–Lifshitz equation for both materials was also set to 0.5, in order to get relatively fast simulations.

It is not straightforward to compare the magnetic properties of an isolated wire with those of a nanowire array. However, an array of nanowires has millions of them, each with lengths in the range of microns, so it is impossible to simulate the experimental system. To overcome this problem, Morales-Concha *et al* [28] proposed a theoretical model that allows to calculate both the magnetostatic interactions and forces between cylindrically shaped particles with different geometrical parameters. They obtained that the stray field of a simple cylinder is most intense at its extremities. Besides, it is important to keep in mind that thinner cylinders interact less strongly with one another than thicker ones do. In this way, what we have done is to simulate the hysteresis curve of an isolated nanowire, with the idea that it serves as a guide for understanding the experimental curves corresponding to a nanowire array, keeping in mind that the magnetostatic interaction between the nanowires of an array can modify not only the coercivity and remanence obtained [29], but also modify the magnetization reversal mechanism of the nanowires.

The magnetic properties of these nanowires will change as a function of the geometrical parameters thereof, as well as the angle at which the external magnetic field is applied. Figure 1 shows the angle θ between the *z*-axis and the applied magnetic field.
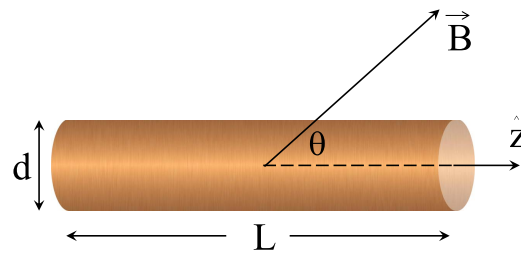
Figure 1. Geometrical parameters of the simulated nanowire and angle at which the external field is applied.
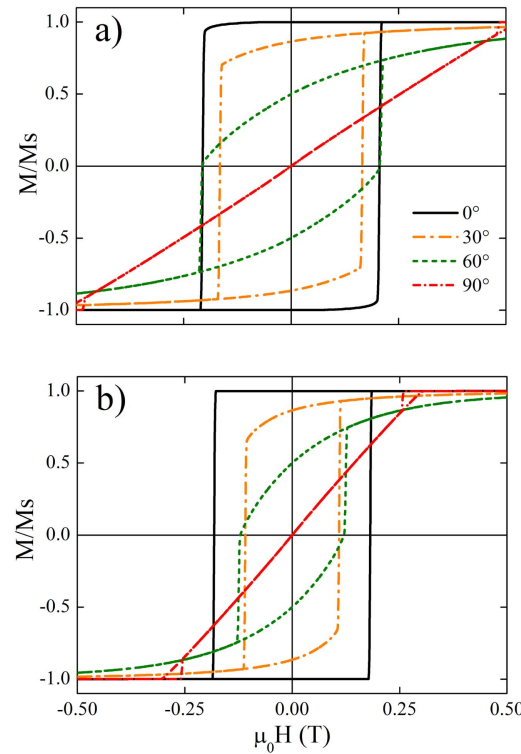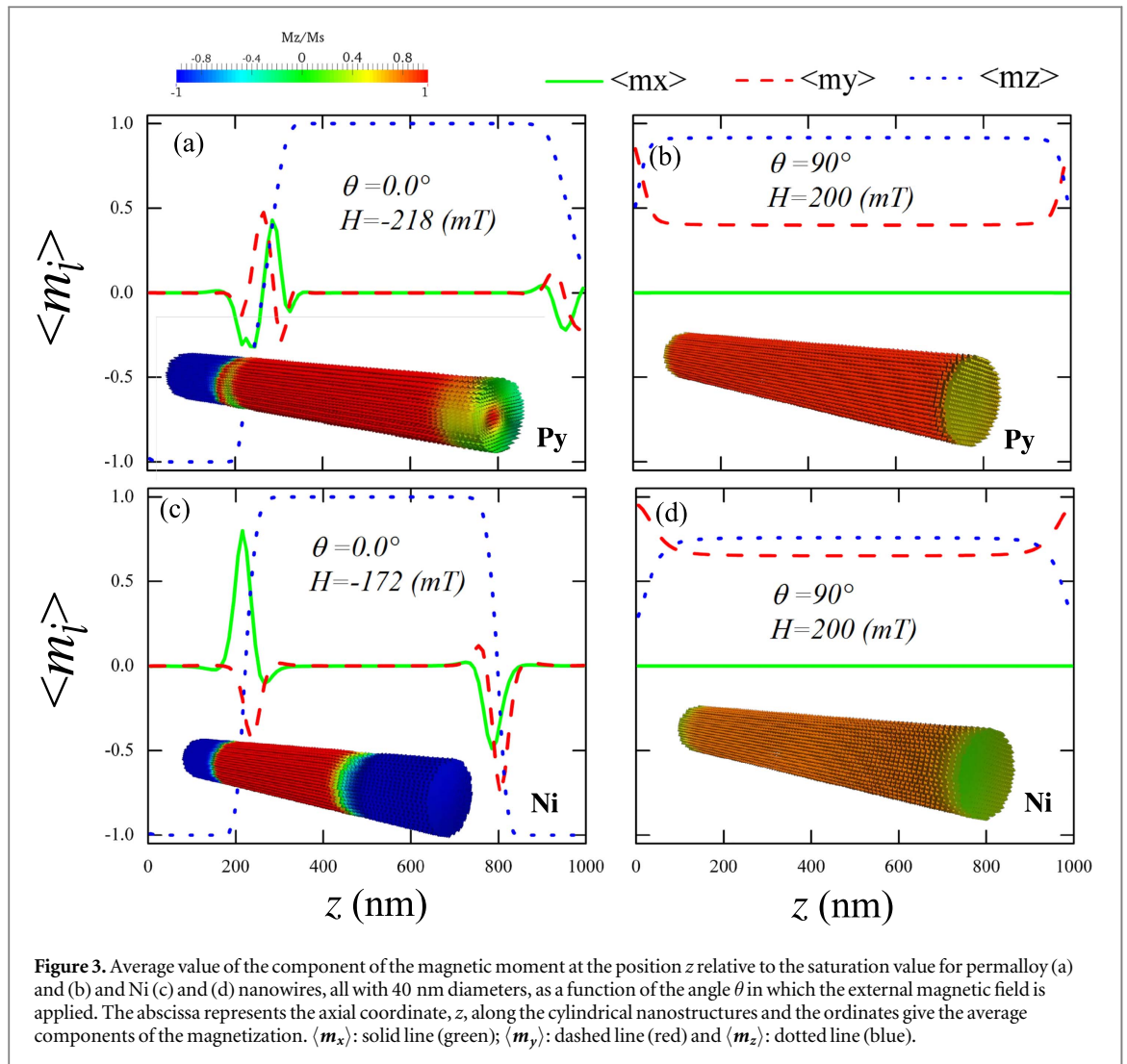

Figure 2. Hysteresis curves for nanowires of (a) permalloy and (b) Ni, both structures with 40 nm diameters, as a function of the angle θ in which the external magnetic field is applied.
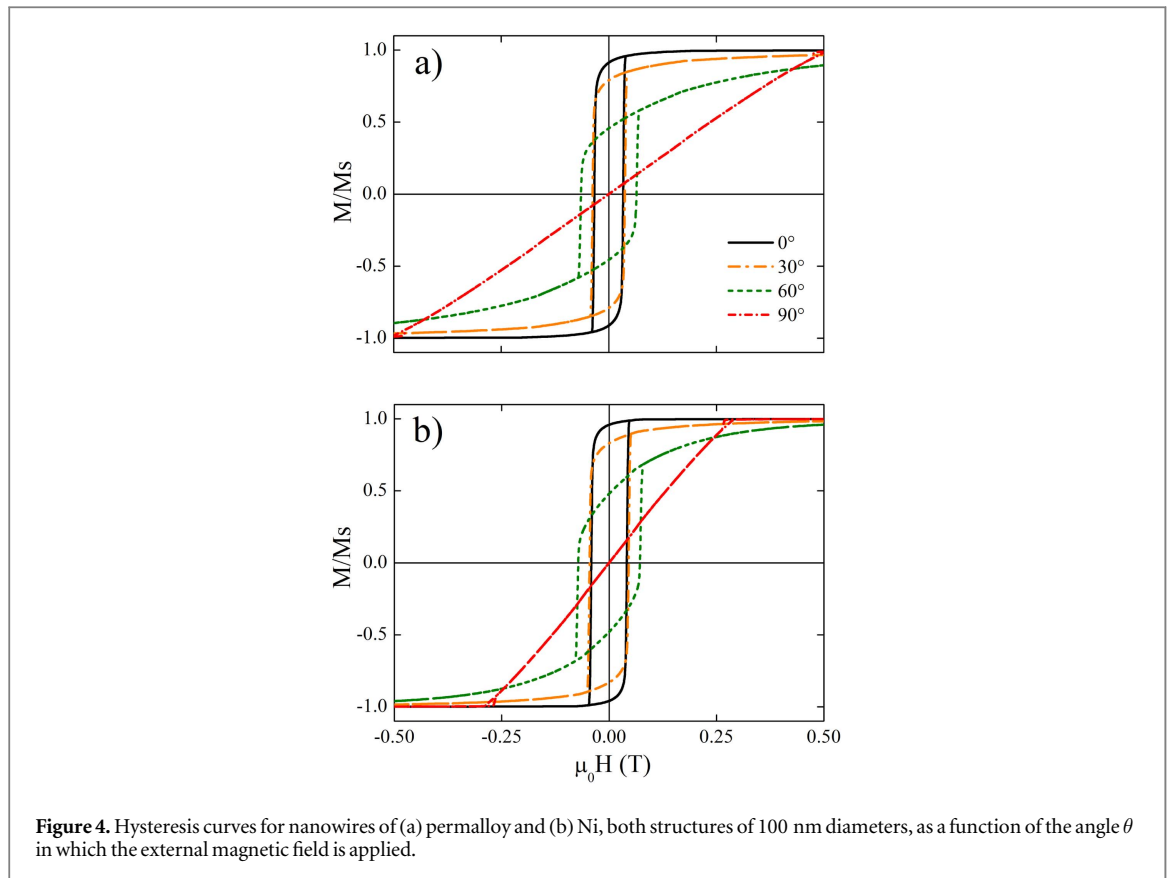
3. Results and discussion

Figure 2 shows the hysteresis curves for a permalloy (a) and a Ni (b) nanowire, both nanostructures of 40 nm diameter and 1 μm long, as a function of the angle θ in which the external magnetic field is applied between 1.0 and -1.0 T (the figures show a lower range for easier viewing). Similar hysteresis curves were obtained by Singh *et al* [30] for an interacting array of permalloy nanowires 40 nm in diameter and 14 μm in length. The differences observed are due to the fact that the numerical simulations consider an isolated wire while the experimental measurements consider an interacting array, so that the magnetostatic interactions between the wires produce a decrease in both the coercivity and the measured remanence. The main aim in this work is to investigate, in a comparative way, the angular dependence of the magnetic properties of permalloy and Ni nanowires, when their diameters and material change. Thus, comparing the NiFe and Ni hysteresis loops depicted in figures 2(a) and (b), respectively, a coercivity 12% higher is observed for a permalloy NW, when the magnetic field is applied in the easy axis of both nanowires, i.e., along the axis of the nanostructures ($\theta = 0°$). Likewise, it is observed that the saturation field for permalloy reaches values that, in percentage, are 11% ($\theta = 0°$) and almost 77% ($\theta = 90°$) higher than the field saturation obtained for a Ni NW, while the remanent magnetization is comparable for both systems, at the same angles. It is worth noting that NiFe hysteresis loops have a more curved shape respect to the Ni ones, which have a pronounced squareness at $\theta = 0°$. It is important to note that coercivity exhibits a non-monotonic behavior with the angle, that is, it decreases from 0° to 30°, then increases from 30° to 60°, and then decreases again between 60° and 90°. On the other hand, remanence decreases with increasing angle. The

Figure 3. Average value of the component of the magnetic moment at the position *z* relative to the saturation value for permalloy (a) and (b) and Ni (c) and (d) nanowires, all with 40 nm diameters, as a function of the angle θ in which the external magnetic field is applied. The abscissa represents the axial coordinate, *z*, along the cylindrical nanostructures and the ordinates give the average components of the magnetization. $\langle m_x \rangle$: solid line (green); $\langle m_y \rangle$: dashed line (red) and $\langle m_z \rangle$: dotted line (blue).

obtained results are a response to the chosen magnetic parameters, which define that the exchange length of the nickel is greater than that of the permalloy.

In order to investigate in more detail the mechanism of magnetization reversal of these NiFe and Ni nanowires of 40 nm diameter, we show snapshots (see figure 3) taken from the hysteresis curve simulated at $\theta = 0°$ and $\theta = 90°$. The nucleation and propagation of a DW (if any) is monitored by the value of $\langle m_i(z) \rangle = \langle M_i(z) \rangle / M_s$, the average value of the component of the magnetic moment at the position *z* relative to the saturation value. Thus, the position of the wall is determined by the maximum of $(1 - |\langle m_z \rangle|)$. The blue line represents the average axial component of the magnetization $\langle m_z \rangle$ while the other two (in-plane) components are given by the green $\langle m_x \rangle$ and red $\langle m_y \rangle$ lines. When the external magnetic field is applied parallel to the axis of NiFe and Ni nanowires ($\theta = 0°$), the $\langle m_x \rangle$ and $\langle m_y \rangle$ components are non-zero, indicating that the wires revert their magnetization by nucleation and propagation of transverse DWs. On the contrary, when the magnetic field is applied perpendicular to the axis of NiFe and Ni nanowires ($\theta = 90°$), the $\langle m_y \rangle$ component decreases steadily throughout the whole wire, except for the covers, giving rise to a pseudo-coherent reversal process.

In figure 4 the hysteresis loops for the two different materials, permalloy (figure 4(a)) and Ni (figure 4(b)), of 100 nm diameter and normalized magnetization are illustrated. In contrast with the previous behavior (see figure 2), a 20% higher coercivity of Ni respect to NiFe is observed when $\theta = 0°$. A slightly increment in the remanent magnetization at $\theta = 0°$ for Ni NWs is observed, while the saturation field is almost 50% lower compared to NiFe nanostructures, at the same angle. It is worth to note a striking behavior that is observed when comparing the hysteresis curves of both permalloy and Ni systems of 100 nm diameters. The coercivity increases with increasing angles between $\theta = 0°$ and $\theta = 75°$ and then drops to zero at $\theta = 90°$. In fact, the high aspect ratio of NW structures explains the *easy axis* that they exhibit along the axis of the wire as well as a difficult magnetization plane, which is perpendicular to the wire axis. Therefore, the wire is easily-magnetizable at $\theta = 0°$, and the magnetic moments tend to keep aligned with the wire axis. So, an intense magnetic field is necessary to modify the moments from this energetically favorable configuration, leading to the exhibition of a

Figure 4. Hysteresis curves for nanowires of (a) permalloy and (b) Ni, both structures of 100 nm diameters, as a function of the angle θ in which the external magnetic field is applied.
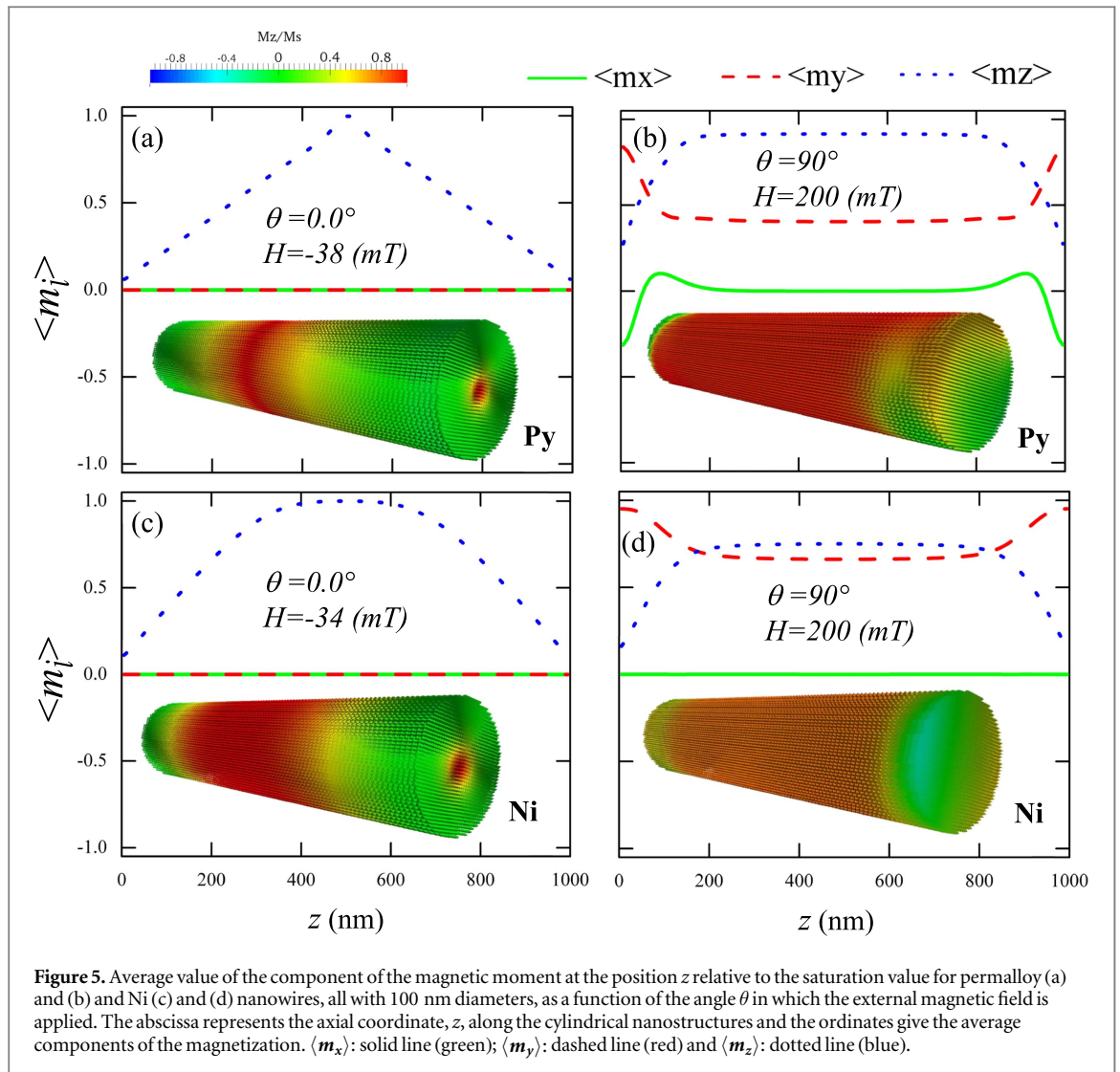
high coercivity. In this case, and observing that the $\langle m_x \rangle$ and $\langle m_y \rangle$ components are zero (see figures 5(a) and (c)), we can conclude that the nanowire reverses its magnetization by nucleation and propagation of vortex DWs.

On the other hand, if the magnetization of the system along an unfavorable direction occurs at $\theta = 90°$, then a little field variation provokes a significant change in the magnetization, due to the magnetic moments tend to stay perpendicular aligned to the applied field, and only a small external magnetic field is enough to modify this configuration. Thus, the exhibition of coercivity is not expected. In this case, the nanowire reverses its magnetization by a pseudo-coherent rotation, where almost all the magnetic moments revert at the same time, as shown in figures 5(b) and (d).

Figure 6 shows the coercivity and remanence as a function of the angle at which the external magnetic field is applied for different materials and diameters. As mentioned above, coercivity exhibits a non-monotonic behavior as a function of θ. It is interesting to note that for small angles, permalloy nanowires with $d = 40$ nm exhibit greater coercivity than nickel ones, while the opposite behavior is obtained for nanowires with $d = 100$ nm. For the permalloy wires the maximum coercivity occurs at 60° ($d = 40$ nm) and 75° ($d = 100$ nm), while for nickel nanowires it occurs at 0° ($d = 40$ nm) and 60° ($d = 100$ nm). From figure 6(a) it is concluded that, for the same material, the coercivity will be lower for those wires with a larger diameter, regardless of the angle in which the external magnetic field is applied [13]. The explanation for this phenomenon is that because in a cylinder with a small diameter the exchange interaction dominates, the system will prefer to keep its magnetization pointing in a single direction, so a very strong external magnetic field will be necessary to start the magnetization reversal process. These systems will exhibit square hysteresis curves (see figure 2), typical of a bistable behavior. On the other hand, as the diameter of the wire increases, the dipolar interaction becomes more important, producing closing domains at the ends of the wire, which facilitate the nucleation and propagation of DWs, thus decreasing the external magnetic field necessary to produce its magnetization reversal. In this case the hysteresis curves are not as square as in the previous case (see figure 4). Finally, remanence decreases monotonically by increasing θ. For $d = 40$ nm the remanence is independent of the material, while for $d = 100$ nm, the remanence of Ni is slightly greater than that of permalloy.

It is important to keep in mind that the physics of the problem lies mainly in the nucleation and propagation of DWs, whose width is related to the diameter of the nanowire, and it is independent of its length (as long as the DW width is smaller than the length of the wire and that we are considering an isolated nanowire). However, in the case of an interacting array of nanowires, the length of these plays a fundamental role on their coercivity [31]. If one assumes that all the wires are uniformly magnetized along their axis, then we can imagine that there will be

Figure 5. Average value of the component of the magnetic moment at the position *z* relative to the saturation value for permalloy (a) and (b) and Ni (c) and (d) nanowires, all with 100 nm diameters, as a function of the angle θ in which the external magnetic field is applied. The abscissa represents the axial coordinate, *z*, along the cylindrical nanostructures and the ordinates give the average components of the magnetization. $\langle m_x \rangle$: solid line (green); $\langle m_y \rangle$: dashed line (red) and $\langle m_z \rangle$: dotted line (blue).

magnetic charges on the cylinder caps. This implies that the closer the caps (situation that occurs for short wires), more interacting will be nanowires, producing an abrupt decrease in coercivity [13].

4. Conclusions

In conclusion, micromagnetic simulations have been performed in order to gain insight into the angular, diameter and composition dependences of the magnetic properties for 1 μm long cylindrical nanostructures with wire morphology. The high aspect ratio of NW structures explains the *easy axis* that they exhibit along the axis of the wire as well as a difficult magnetization plane, which is perpendicular to the wire axis. Coercivity exhibits a non-monotonic behavior as a function of θ, while remanence decreases monotonically by increasing θ. For small angles, permalloy nanowires of 40 nm diameters exhibit greater coercivity than nickel ones, while the opposite behavior is obtained for nanowires of 100 nm diameters. For $d = 40$ nm the remanence is independent of the material, while for $d = 100$ nm, the remanence of Ni is slightly greater than that of permalloy. These results allow to conclude that both the magnetic (material) and the geometric (diameter) parameters play a fundamental role when defining the magnetic properties of the nanowires.

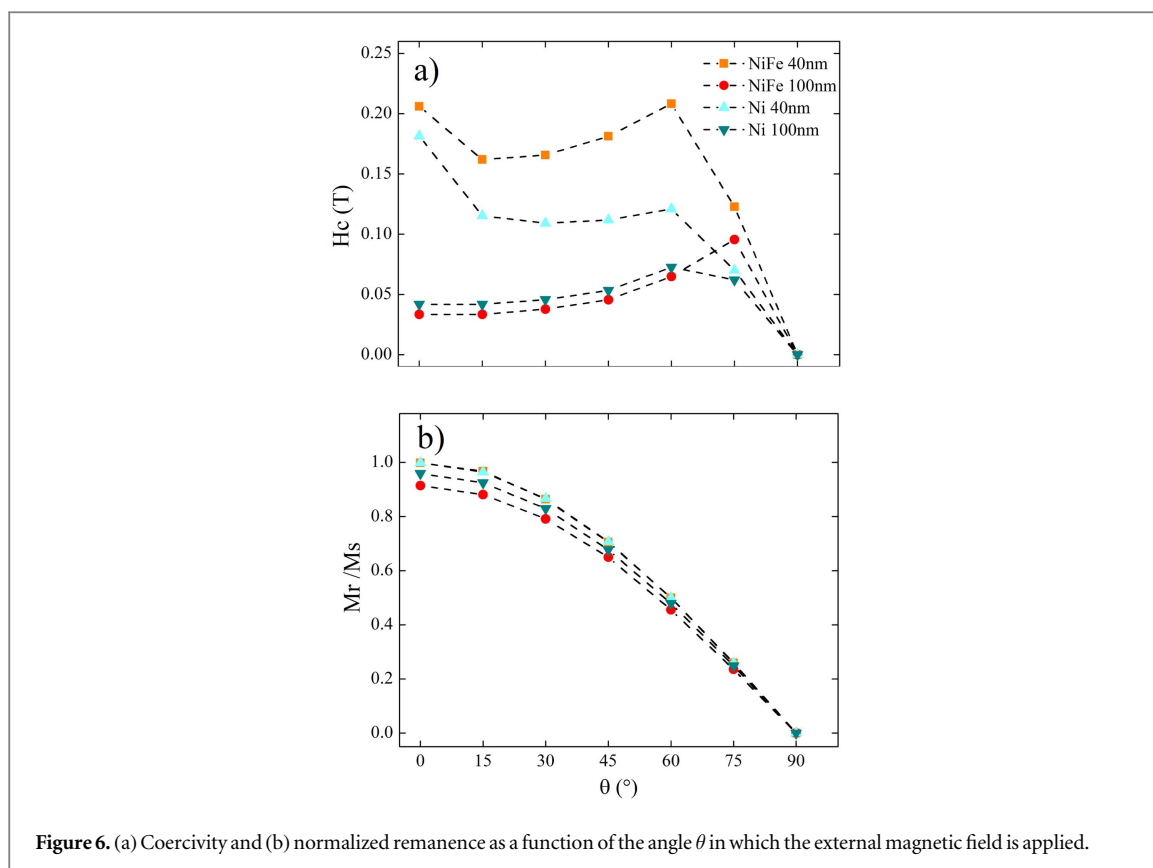## Acknowledgments

Figure 6. (a) Coercivity and (b) normalized remanence as a function of the angle θ in which the external magnetic field is applied.

ORCID iDs

Juan Escrig ⬤ https://orcid.org/0000-0002-3958-8185

References

[1] Goolaup S, Ramu M, Murapaka C and Lew W S 2015 *Sci. Rep.* **5** 9603
[2] Maurer T, Ott F, Chaboussant G, Soumare Y, Piquemal J Y and Viau G 2007 *Appl. Phys. Lett.* **91** 17250
[3] Reich D H, Tanase M, Hultgren A, Bauer L A, Chen C S and Meyer G J 2003 *J. Appl. Phys.* **93** 7275–80
[4] Sellmyer D, Zheng M and Skomski R 2001 *J. Phys. Condens. Matter* **13** R433–60
[5] Nguyen T M and Cottam M G A 2004 *J. Magn. Magn. Mater.* **272–276** 1672–3
[6] Pereira A, Gallardo C, Espejo A, Briones J, Vivas L, Vázquez M, Denardin J and Escrig J 2013 *J. Nanopart. Res.* **15** 2041
[7] Ivanov Y P, Chuvilin A, Lopatin S and Kosel J 2016 *ACS Nano* **10** 5326–32
[8] Currivan J A, Youngman J, Mascaro M D, Baldo M A and Ross C A 2012 *IEEE Mag. Lett.* **3** 3000104
[9] Shapira E, Tsukernik A and Selzer Y 2007 *Nanotechnology* **18** 485703
[10] Bohnert T, Vega V, Michel A-K, Prida V M and Nielsch K 2013 *Appl. Phys. Lett.* **103** 092407
[11] Chandra Sekhar M, Liew H F, Purnama I, Lew W S, Tran M and Ha G C 2012 *Appl. Phys. Lett.* **101** 152406
[12] Lavín R, Denardin J C, Escrig J, Altbir D, Cortés A and Gómez H 2009 *J. Appl. Phys.* **106** 103903
[13] Escrig J, Lavín R, Palma J L, Denardin J C, Altbir D, Cortes A and Gomez H 2008 *Nanotechnology* **19** 075713
[14] Lavin R, Denardin J C, Espejo A P, Cortés A and Gómez H 2010 *J. Appl. Phys.* **107** 09B504
[15] Singh A K, Das B, Sen P, Bandopadhyay S K and Mandal K 2014 *IEEE Trans. Magn.* **50** 2302104
[16] Salem M S, Sergelius P, Corona R M, Escrig J, Goerlitz D and Nielsch K 2013 *Nanoscale* **5** 3941
[17] Zhu H, Yang S G, Ni G, Tang S L and Du Y W 2001 *J. Phys. Condens. Matter* **13** 1727
[18] Martin C R 1994 *Science* **266** 1961–6
[19] Alikhani M, Ramazani A, Almasi Kashi M, Samanifar S and Montazer A H 2016 *J. Magn. Magn. Mater.* **414** 158–67
[20] Zhang X, Zhang H, Tianshan W and Hui-Yuan S 2013 *J. Magn. Magn. Mater.* **331** 162–7
[21] Vorobjova A, Dmitry L S, Kazimir I Y, Prischepa S L and Outkina E A 2016 *Beilstein J. Nanotechnol.* **7** 1709–17
[22] Salem M S, Sergelius P, Zierold R, Moreno J M M, Goerlitz D and Nielsch K 2012 *J. Mater. Chem.* **22** 8549–57
[23] Aravamudhan S, Singleton J, Goddard P and Bhansali S 2009 *J. Phys. D: Appl. Phys.* **42** 115008
[24] Willcox M, Ding A and Xu Y 2012 *J. Nanosci. Nanotechnol.* **12** 6484–7
[25] Leighton B, Pereira A and Escrig J 2012 *J. Magn. Magn. Mater.* **324** 3829–33
[26] Gilbert T L 1955 *Phys. Rev.* **100** 1243
[27] Donahue M J and Porter D G 2002 *OOMMF User's Guide, Version 1.2 a3* http://math.nist.gov/oommf
[28] Morales-Concha C, Ossandón M, Pereira A, Altbir D and Escrig J 2012 *J. Appl. Phys.* **111** 07D131
[29] Lavín R, Gallardo C, Palma J L, Escrig J and Denardin J C 2012 *J. Magn. Magn. Mater.* **324** 2360–2
[30] Singh A K, Khan G G, Das B and Mandal K 2016 *J. Nanosci. Nanotechnol.* **16** 994–7
[31] Singh A K and Mandal K 2014 *J. Nanosci. Nanotechnol.* **14** 5036–41